Cell Reports
Physical Science

CellPress
OPEN ACCESS

Article

Adaptive helicity and chiral recognition in bright europium quadruple-stranded helicates induced by host-guest interaction

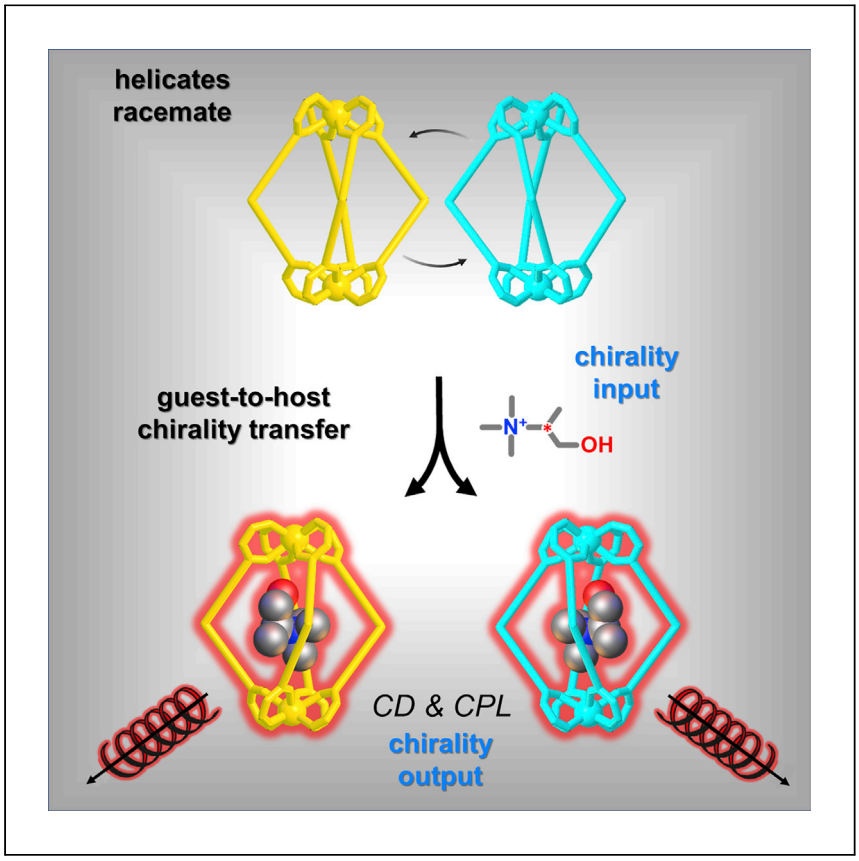

Rancan et al. report chirality transfer for chiroptical molecular recognition. Very bright europium helicates enable a chiroptical readout toward chiral guests. Helicates adapt their conformation with a guest-to-host hierarchical chirality transfer. The molecular recognition process is detected by induced circular dichroism (CD) and circularly polarized luminescence (CPL).

Marzio Rancan, Jacopo Tessarolo, Alice Carlotto, ..., Maurizio Casarin, Guido H. Clever, Lidia Armelao

marzio.rancan@cnr.it (M.R.)
jacopo.tessarolo@tu-dortmund.de (J.T.)

Highlights

Helicates adapt in response to a recognition process in a confined space

Chiral recognition through host-guest events detected by CD and CPL

Very bright europium helicates with luminescence visible to naked eye

Helicity inversion mechanism, i.e., Bailar twist, is revealed by DFT calculations

Rancan et al., Cell Reports Physical Science 3, 100692
January 19, 2022
https://doi.org/10.1016/j.xcrp.2021.100692

Cell Reports
Physical Science

CellPress
OPEN ACCESS

Article

Adaptive helicity and chiral recognition in bright europium quadruple-stranded helicates induced by host-guest interaction

Marzio Rancan,[1,6,*] Jacopo Tessarolo,[2,*] Alice Carlotto,[3] Silvia Carlotto,[1,3] Maria Rando,[3] Lucrezia Barchi,[3] Elisa Bolognesi,[3] Roberta Seraglia,[4] Gregorio Bottaro,[1] Maurizio Casarin,[3] Guido H. Clever,[2] and Lidia Armelao[3,5]

SUMMARY

Chiral information transfer is crucial to design new functions like, for instance, sensing through chiroptical probes in which the input is readout as a consequence of a chiral recognition event. Herein, we report lanthanide quadruple-stranded helicates $[Ln_2L_4]^{2-}$ that show a guest-to-host chirality transfer. As confirmed by X-ray diffraction (XRD) and density functional theory (DFT) calculations, these cages are present in solution as an equilibrating racemic mixture of left- and right-handed helicates. The helicates adapt their helical conformation by encapsulation of a chiral guest enabling also straightforward enantiomeric excess determination. Asymmetric induction is demonstrated by circular dichroism (CD) and circularly polarized luminescence (CPL), and a helicity inversion mechanism based on a Bailar twist is proposed and studied by DFT calculations. The presented research contributes to the design of helicates with a unique combination of confined cavities, adaptive chirality, and peculiar luminescent properties, finding applications toward the development of optical probes for selective chiral sensing via molecular recognition.

INTRODUCTION

Chemists know that chirality can manifest at hierarchical level, and many efforts are devoted to study and control the transmission of chiral information through space and across length scales.[1] At a primary molecular level, chirality can be imposed via stereocenters. However, chirality can originate at a secondary level even through the combination of achiral building blocks such as metal ions and ligands to give discrete or extended systems with propeller (Λ/Δ) or helical (M/P) structures.[2–4] Among metallo-supramolecular systems, helicates, i.e., architectures where organic ligands wrap around two or more metal ions with a helical twist,[5–7] are a paradigmatic example of chirality at a secondary level. In absence of a source of "hard" chirality, achiral components self-assemble to give a racemic mixture of left- and right-handed helicates, and in some cases an achiral structure called mesocate.[8] The possibility to control the system helicity trough supramolecular interactions with an external source of absolute chirality is very appealing, paving the way to systems that can be exploited for hierarchical chirality transfer and for chiral sensing via molecular and supramolecular recognition events. Asymmetrization of helicates racemic mixtures has been reported using chiral counterions to select one specific enantiomer.[9,10] More interestingly, for helicates assemblies with accessible cavities,

[1]Institute of Condensed Matter Chemistry and Technologies for Energy (ICMATE), National Research Council (CNR), c/o Department of Chemistry, University of Padova, via F. Marzolo 1, 35131 Padova, Italy

[2]Department of Chemistry and Chemical Biology, TU Dortmund University, 44227 Dortmund, Germany

[3]Department of Chemical Sciences, University of Padova, via F. Marzolo 1, 35131 Padova, Italy

[4]Institute of Condensed Matter and Technologies for Energy (ICMATE), National Research Council (CNR), Corso Stati Uniti, 4, 35127 Padova, Italy

[5]Department of Chemical Sciences and Materials Technologies (DSCTM), National Research Council (CNR), Piazzale A. Moro 7, 00185 Rome, Italy

[6]Lead contact

*Correspondence: marzio.rancan@cnr.it (M.R.), jacopo.tessarolo@tu-dortmund.de (J.T.)

https://doi.org/10.1016/j.xcrp.2021.100692

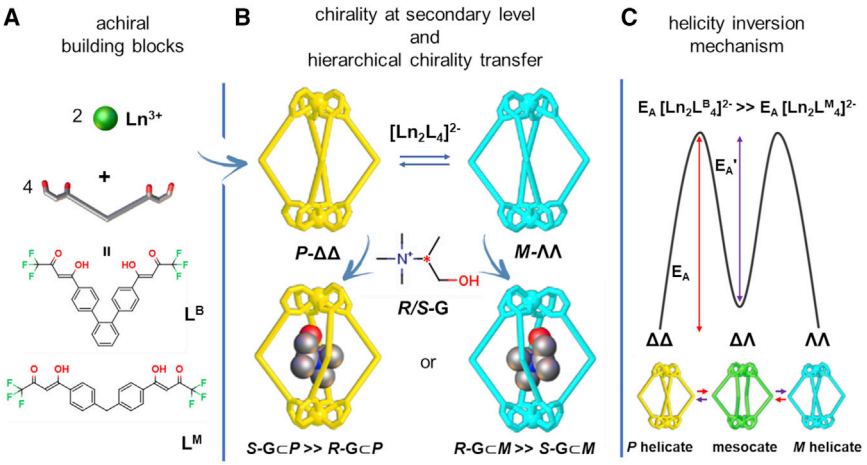

Figure 1. Schematic illustration of the chirality transfer and the helicity inversion mechanism

(A) Achiral building blocks: Ln^{3+} ions and ligands L^B and L^M.

(B) Self-assembly of a racemic mixture of quadruple-stranded helicate-cages and hierarchical chirality transfer from the chiral guest to the host.

(C) Bailar twist-based helicity inversion with activation energies related to the ligand nature.

it is possible to study host-guest interaction with chiral molecules, thus modulating the ratio of the two enantiomers and exploiting a guest-to-host chirality transfer.[11–15]

Recently, introduction and transfer of chiral information among metal-mediated supramolecular assemblies has been expanded by using lanthanide (Ln) metal centers.[16] These systems allow to combine the chiral input with the peculiar lanthanide optical properties, obtaining chiroptical output such circular dichroism (CD) and strong circularly polarized luminescence (CPL), opening up applications ranging from new optically active materials to chiral biosensing and imaging[16–23] in consideration also of the fact that the interaction with biomolecules and DNA have been extensively studied for transition-metal-based helicates.[24–28] Optical probes based on CPL provide the access to a unique chiroptical output, overcoming possible overlap with the detected substrate. Optically pure lanthanide helicates[29–46] are usually prepared by introducing chiral polytopic ligands or even chiral ancillary ligands. Even though brilliant strategies are developing, in most of the reported lanthanide-based helicates a homochiral moiety, with consequent synthetic effort, is necessary to isolate optically pure compounds. Helicates self-assembled from achiral components require straightforward synthetic approach and can show interesting properties such as dynamic and adaptive helicity reorganization as a consequence of a chiral recognition event.[11–15] Here, we couple this feature to host-guest properties and to europium (Eu^{3+}) ions peculiar emission in order to exploit a chiroptical readout (CD and CPL) of the chiral recognition event. We report lanthanide-based quadruple-stranded helicates of formula $[Ln_2L_4]^{2-}$ (Ln = La^{3+}, Eu^{3+}, Gd^{3+}; L = L^B, L^M), self-assembled from achiral components (Figure 1A). Remarkably, introduction of a chiral guest allows to control the equilibrium of the helicates racemic mixture, selecting either the *M* or *P* isomers via a guest-to-host chirality transfer (Figure 1B) and enabling also straightforward enantiomeric excess determination of the guest.

A combination of single-crystal X-ray diffraction (SCXRD), mass spectrometry (MS), NMR analysis, and density functional theory (DFT) calculations was used to study the cages and their host-guest properties with chiral and achiral guests. When using

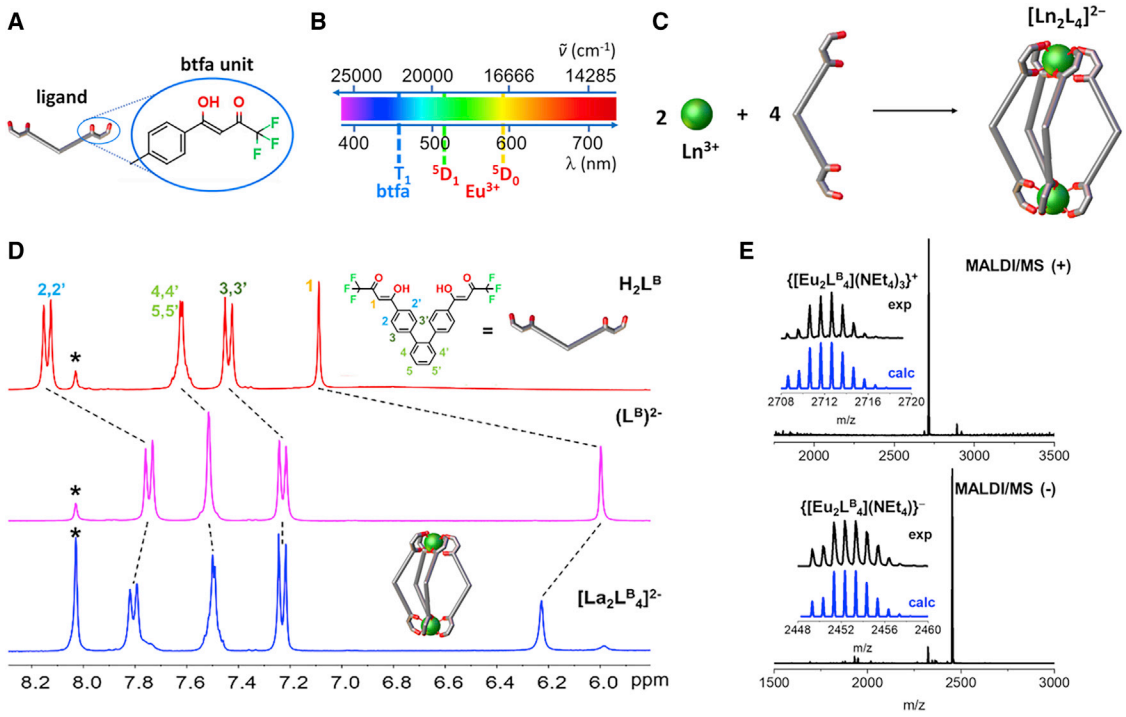

Figure 2. Synthesis and characterization of cages $[Ln_2L_4]^{2-}$

(A) Schematization of the binding unit of ligands L^B and L^M.

(B) Energies of the states involved in the antenna process for btfa (T_1 = 21,470 cm^{-1})[51] and Eu^{3+} ($^5D_1$ = 18,973 cm^{-1} and $^5D_0$ = 17,227 cm^{-1}).[53]

(C) Formation of a lantern-like cage $[Ln_2L_4]^{2-}$.

(D) ^{1}H-NMR spectra (25°C, 200 MHz, DMF-d_7) of protonated ligand H_2L^B, deprotonated ligand $(L^B)^{2-}$, and cage $[La_2L^B_4]^{2-}$, * represents DMF.

(E) MALDI/MS in positive and negative mode for $\{[Eu_2L^B_4](NEt_4)_2\}$. Inset: Experimental (black) and calculated (blue) isotopic patterns for the main peaks.

Eu^{3+}, the helicates show intense emission and very high brightness, a property that represents an interesting parameter for applications in luminescent microscopy and bioimaging.[47–50] Furthermore, the chiroptical properties of Eu cages allows to study the guest-to-host chiral induction not only by CD spectroscopy but also by CPL analysis, proving that the chiral information is transferred to both backbone and coordination environment of the helicate. The system response to the guest-to-host asymmetrization is affected by the host-guest affinities. An intramolecular mechanism via Bailar twist for the helicity inversion was proposed and studied by DFT calculations, which demonstrated that the ligand nature (flexibility versus rigidity) plays a crucial role on the activation energy of the intramolecular helicate twisting mechanism (Figure 1C), allowing to rationalize guidelines for the design of such functional helicates.

RESULTS AND DISCUSSION

Cage synthesis and characterization

We designed two bis-β-diketone ligands, L^B and L^M, characterized by two homotopic coordination sites that correspond to btfa (benzoyltrifluoroacetone) units, connected by two different central scaffolds, varying in flexibility, with a 2-fold axis passing through the ligand center (Figure 1). β-Diketone derivatives bearing a btfa group are reported in literature as good sensitizers for Eu^{3+} ions (Figures 2A and 2B).[51] Ligands were synthesized using a two-step protocol:[52] (1) a Friedel-Crafts acylation followed by (2) a Claisen condensation and characterized as described in the supplemental information (Figures S1–S12). The two ligands were also characterized by SCXRD (Figure S22).

Tetrakis-[Ln(β-diketonate)$_4$]$^-$ complexes usually prefer an octa-coordination mode with a square antiprismatic (SAPR-8) geometry (Figure S13A). By combining the trivalent ions in a local D_{4d} (C_4-axis) symmetry, imposed by the four β-diketonates, with a ligand possessing a C_2-axis, according to the symmetry interaction approach,[54] it is possible to design a lantern-like cage with general formula $[Ln_2L_4]^{2-}$ (Figure 2C). The synthesis of the cages is straightforward. An ethanol solution of a Ln^{3+} salt is added dropwise to a stirred ethanol solution of the deprotonated ligand, and the formation of a precipitate is observed. By using a metal:ligand:base molar ratio equal to 1:2.5:5, the pure cages in high yield were obtained (Table S1). The protonated base acts as countercation for the negatively charged $[Ln_2L_4]^{2-}$ cage. Best results in terms of solubility are obtained using NEt_4^+ (tretraethylammonium) and $DCHA^+$ (dicyclohexylamonium). The analogs lanthanum cages have been assembled for NMR characterization ($DCHA^+$ as counterion). Upon deprotonation, all the ligand signals undergo upfield shifting, with the strongest effect on the proton H1, in α position of the β-diketonate moiety, shifting from ca. 7.1 to ca. 5.9 ppm. After La^{3+} coordination, both H1 and H2, the two signals closer to the metal center, are downfield shifted, as commonly observed after metal coordination (Figure 2D). Analogous results were observed for the cage $[La_2L^M_4]^{2-}$, where the backbone higher flexibility resulted in a broader spectrum (Figure S14). MS analyses confirmed the formation of the desired products. Positive and negative MALDI/MS spectra for $\{[Eu_2L^B_4](NEt_4)_2\}$ are reported in Figure 2E. Similar results were obtained for the cage $\{[Eu_2L^M_4](NEt_4)_2\}$ (Figure S15). Electrospray ionization ESI/MS spectra for all the prepared cages are reported in supplemental information (Figures S16–S21; Table S2).

The cage assembly and structure for the Eu-based cages has been ultimately confirmed by SCXRD (Figures S23–S26 and Table S3). Single crystals of $\{[Eu_2L^B_4](NEt_4)_2\}$ were obtained by slow reactants diffusion: ligand L^B was dissolved in chloroform, layered with a dichloromethane buffer layer, and then with a methanol solution of the europium salt ($EuCl_3 \cdot 6H_2O$) and the base (NEt_4OH). Single crystals for $\{[Eu_2L^M_4](NEt_4)_2\}$ were obtained from acetonitrile by slow solvent evaporation. The crystal structures of the two cages show the presence of two Eu^{3+} ions tetrakis-chelated by the β-diketonato groups of four ligands, to form a lantern-like structure as designed (Figures 3A and 3B). A stereochemical study of the eight-coordinated Eu centers based on a continuous shape measures analysis[55] (see supplemental experimental procedures for details; Tables S6 and S7) shows that in $\{[Eu_2L^M_4](NEt_4)_2\}$ the Eu coordination geometry is very close to an ideal SAPR-8, while for $\{[Eu_2L^B_4](NEt_4)_2\}$ it is more distorted. The Eu–O distances are all similar (Tables S4 and S5), in the range of 2.361–2.409 Å for $\{[Eu_2L^B_4](NEt_4)_2\}$ and 2.392–2.401 Å for $\{[Eu_2L^M_4](NEt_4)_2\}$. The maximum distance between the opposite ligand spacers is 14.9 Å for the cage with L^B-based cage and 12.9 Å for L^M-based cage. In both cases, this distance is higher than the Eu···Eu distance: 10.9 Å for $\{[Eu_2L^B_4](NEt_4)_2\}$ and 11.8 Å for $\{[Eu_2L^M_4](NEt_4)_2\}$. The cage with ligand L^B has a more squashed structure. The crystal structures highlight that one of the two NEt_4^+ counterions is allocated inside the cavity, suggesting host-guest properties for these systems. The hosting of the NEt_4^+ ion inside the cavity is favored not only by charge complementarity but also by specific interactions between the guest and the host. The NEt_4^+ molecule inside the cavity interacts with the cage via Eu–O···H–C interactions, with an average distance of 2.6 Å. Similar Eu–O···H–C and C–F···H–C interactions are observed also for the NEt_4^+ ion outside of the cavity, with an average distance for both types of interactions of 2.7 Å. In fact, in the solid state, the crown formed by four CF_3 terminal groups acts as binding unit for the external NEt_4^+. The two cages have very similar structures. However, the way in which the four ligands wrap around the two Eu ions induces an important difference. In $\{[Eu_2L^B_4](NEt_4)_2\}$, the two metal ions have the same helicity and the cage

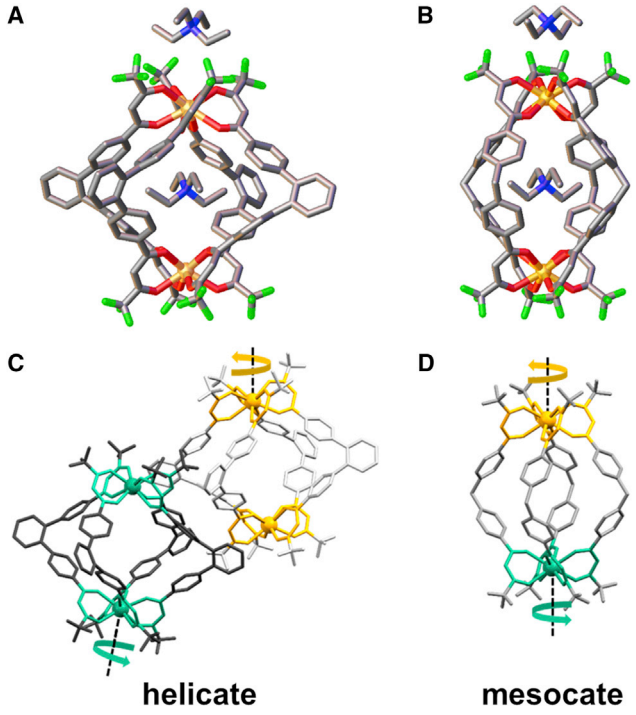

Figure 3. X-ray crystal structures

(A and B) Crystal structures of $\{[Eu_2L^B_4](NEt_4)_2\}$ (A) and $\{[Eu_2L^M_4](NEt_4)_2\}$ (B). Color code: C, gray; O, red; N, blue; F, green; Eu, light orange. H atoms omitted for clarity.

(C and D) Helicates *M* and *P* in $\{[Eu_2L^B_4](NEt_4)_2\}$ (C) and mesocate for $\{[Eu_2L^M_4](NEt_4)_2\}$ (D), where the helicity of the metal centers is highlighted with different colors: green (Λ) and yellow (Δ). H atoms and NEt_4^+ ions omitted for clarity.

is a dinuclear quadruple-stranded helicate. In the unit cell, both the right-handed (*P*, $\Delta\Delta$) and left-handed (*M*, $\Lambda\Lambda$) helicates are present in 1:1 ratio (Figure 3C). The two helicates interact through C–F···H–C interactions, resulting in a supramolecular couple. On the other hand, in $\{[Eu_2L^M_4](NEt_4)_2\}$, the two metal ions have opposite helicity ($\Delta\Lambda$) and the cage is a dinuclear quadruple-stranded mesocate (Figure 3D). The Eu centers helicity is highlighted in Figures 3C and 3D.

Photophysical studies

Emission spectra of the Gd cage analogs (Figures S27A and S27B), recorded at room and low (77 K) temperature, were used to derive ligand triplet (T_1) energies. The T_1 values are only slightly affected by the different ligand spacers and close to the btfa energy[51] (21,470 cm^{-1}): 21,300 cm^{-1} for L^M and 20,400 cm^{-1} L^B. Absorption spectra of free ligands and the Eu cages are reported in Figures S27C and S28 along with cages excitation spectra (Figure S27D). The similar profiles confirm a ligand-centered excitation. Photoluminescence (PL) spectra (Figure 4A) of the two Eu cages are similar and dominated by the hypersensitive transition ($^5D_0 \rightarrow {}^7F_2$, 612 nm), whose intensity is about one order of magnitude higher than what observed for the other transitions ($^5D_0 \rightarrow {}^7F_J$, J = 0, 1, 3, and 4). Similar profiles have been found in other Eu-β-diketonates.[53,56,57] The cages solutions when irradiated with a UV source show an intense red luminescence (Figure 4B). Remarkably, the brightness of these Eu cages is high enough to ensure a visible luminescence even to the naked eye in daylight when the compounds are simply exposed to the sunlight (Figure 4C). The brightness values are 57,460 and 43,750 $M^{-1}\cdot cm^{-1}$ for $[Eu_2L^B_4]^{2-}$ and $[Eu_2L^M_4]^{2-}$, respectively. Table S8 reports the molar extinction coefficients (ε_{max}), the

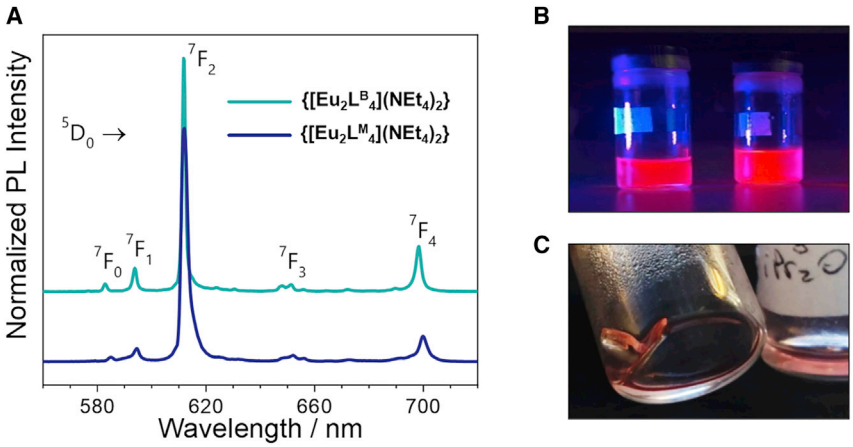

Figure 4. Cages emission

(A) Room temperature photoluminescence spectra for the Eu cages (λ_{ex} = 330 nm) in CH_3CN.
(B) Eu cages solutions (CH_3CN) red emission upon UV-light excitation (λ_{ex} = 365 nm).
(C) Images of the red luminescence of {[$Eu_2L^M_4$](NEt_4)$_2$} single crystals exposed to sunlight.

absolute photoluminescence quantum yield (PLQY), and the brightness (B = PLQY·ε) for the two cages.

Host-guest studies

SCXRD structures evidenced that both the cages have a cavity suitable to host small molecules such as NEt_4^+. For this reason, we decided to investigate guest binding of positively charged tetralkylamonium ions, the achiral NEt_4^+ and the chiral α-methylcholine (*R*-G and *S*-G), with $[La_2L^B_4]^{2-}$ and $[La_2L^M_4]^{2-}$ cages. The chiral guest is a choline derivative. Choline, acethylcholine, methylcholine, and carnitine play important roles in biological systems. In particular, (*R*)-α-methylcholine is an inhibitor of the choline transport system with a much higher effect than the (*S*)-α-methylcholine enantiomer. $DCHA^+$ was used as counterion, to ensure an empty inner space, since this ion is too big to be hosted in the cage's cavity. The systems were studied by ^{1}H-NMR, and the formation of the host-guest species could be easily followed looking at the diagnostic α proton (H1) of the β-diketone moiety and at the guest signals (Figure 5). For both cages, addition of NEt_4Cl results in two sets of signals, one belonging to the empty cages and the other to the host-guest species, suggesting a slow exchange scenario (Figures 5A and 5B; Figures S29–S31). Furthermore, the signals relative to the terminal methyl groups of the guests are downfield shifted, proving the interaction with the inner cavity (−0.50 and −1.58 ppm for {$NEt_4\subset[La_2L^B_4]$}$^-$ and {$NEt_4\subset[La_2L^M_4]$}$^-$, respectively). When using the chiral α-methylcholine, $[La_2L^B_4]^{2-}$ cage showed a fast host-guest equilibrium (Figure 5C), indicated by shifting of the cage protons. Differently, $[La_2L^M_4]^{2-}$ showed a slow exchange at the NMR timescale, evidencing at low ppm (<0.5) the signal relative to the encapsulated guest (Figure 5D; Figures S29 and S30). Again, spectra revealed two sets of signals related to the empty cage and to the host-guest species. Association constants for slow exchange systems were derived by using an internal standard (supplemental information) and by NMR titration for fast exchange (Figures S32–S35). Diffusion-ordered spectroscopy (DOSY) analysis on both empty and host-guest cages supports the encapsulation, with an increase of the hydrodynamic radius of about 2 Å for the filled cages (Figure S36; Table S9). Table 1 reports the calculated values for all the host-guest species. In general, $[La_2L^M_4]^{2-}$ binds the guests stronger than $[La_2L^B_4]^{2-}$, and NEt_4^+ is bound stronger than *R*/*S*-G. As expected, the guests *R*-G and *S*-G show association constant very close in value.

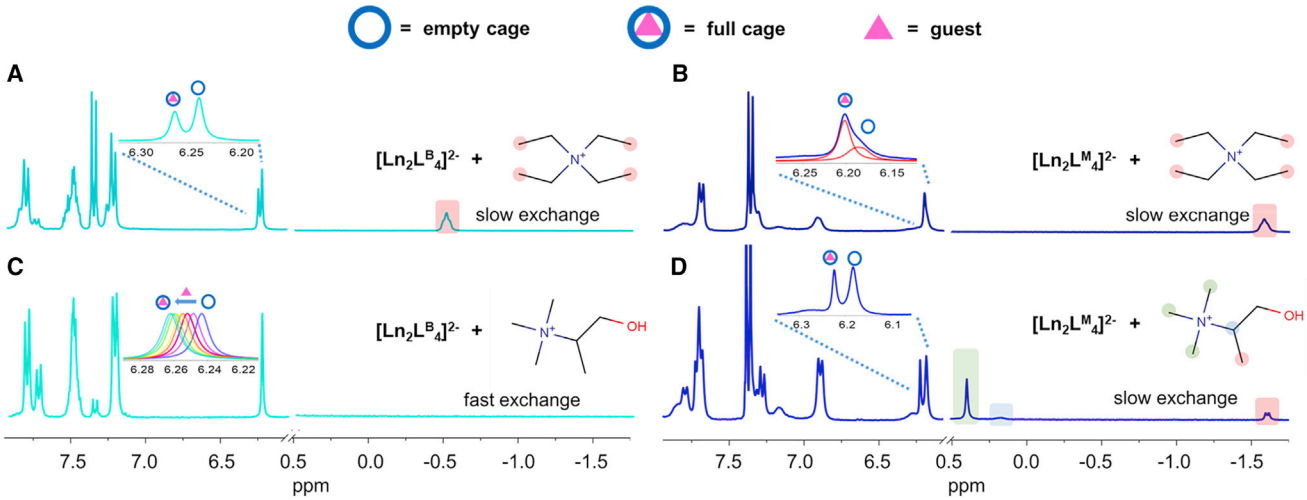

Figure 5. ^{1}H-NMR of the host-guest species

(A–D) 1H-NMR spectra (25°C, 300 MHz, DMF-d_7) of the host-guest systems with achiral and chiral guests. Guest equivalents (eq): 1.0 eq of NEt_4^+ (A), 1.0 eq of NEt_4^+ (B), from 0 to 50 eq of *S*-G (C), and 0.5 eq of *S*-G (D). Spectra with *R*-G are reported in supplemental information (Figures S29, S30, and S34).

Supramolecular chirality transfer

Considering both the host-guest and chiral properties of the helicate-cages, we investigated the possibility to couple these supramolecular properties. As stated above, such multiple-stranded helicates, in absence of chiral information, exist in solution as a racemic mixture of *P*- and *M*-helicates, and possibly as the mesocate isomer; thus, they are optically inactive. Enantiomeric enrichment can be induced by host-guest interactions, resulting in display of chiroptical properties such CD and CPL.

Either chiral guests (*R*-G and *S*-G) or cages (gray line, Figure 6) do not show CD signals in the considered wavelength ranges (270–380 or 280–400 nm). Nevertheless, with the addition of the chiral guest to the cages solution an induced CD (ICD) signal was observed in the cage's absorption region (dashed line, Figures 6A and 6B; Figure S37; Table S10).[13] The two Eu cages showed similar CD spectra. In particular, all the systems evidence one positive and one negative Cotton effect. It is well known that when two or more identical chromophores are in close proximity with a chiral disposition, exciton coupling can produce bisignate CD curves, named exciton couplets.[32,33,58,59] The so-called Davydov splitting[60] is 33 nm for both $[Eu_2L^M{}_4]^{2-}$ and $[Eu_2L^B{}_4]^{2-}$ cages either with *R*-G or *S*-G chiral guest. There is a strong and well-documented[59] correlation between the absolute configurations of the metal ion and the couplet signs. The sign is indicated as positive when the exciton couplet has a positive amplitude at lower energy and negative when it displays the opposite situation. In particular, Λ configuration is associated to a positive exciton couplet, while a negative exciton couplet is related to the Δ configuration. In both cages, *R*-G induces a positive couplet, while *S*-G promotes the formation of a negative couplet. This suggests that *R*-G preferentially binds the $\Lambda\Lambda$ or *M*-helicate contrary to *S*-G that preferentially stabilizes the $\Delta\Delta$ or *P*-helicate. All the spectra show an increase of the ICD signal with guest concentration, suggesting that the more the cage encapsulates the chiral guest, the more helicity asymmetrization is induced (Figures 6C and 6D). The effect of temperature on ICD spectra was also evaluated. All the samples show a clear increase of the CD signal by decreasing the temperature, and the variation of the CD signal has a nearly linear trend (Figures S38 and S39). Since it can be postulated that when

Table 1. Association constants for the host-guest systems

	K [M^{-1}] (%)
$\{NEt_4 \subset [La_2L^B_4]\}^-$	$1.3 \cdot 10^3 \pm 9$
$\{NEt_4 \subset [La_2L^M_4]\}^-$	$2.4 \cdot 10^4 \pm 8$
$\{R\text{-}G \subset [La_2L^B_4]\}^-$	14 ± 3
$\{S\text{-}G \subset [La_2L^B_4]\}^-$	18 ± 2
$\{R\text{-}G \subset [La_2L^M_4]\}^-$	709 ± 12
$\{S\text{-}G \subset [La_2L^M_4]\}^-$	694 ± 13

lowering the temperature, the helicity inversion is unfavored, the CD signal enhancement can be attributed to the guest presence in the host inner cavity, in agreement with what previously observed with Pd(II) helicates.[14] The cage with the more flexible ligand L^M responds to lower guest concentrations. Hence, $[Eu_2L^M_4]^{2-}$ has been used for further tests. First, to a $[Eu_2L^M_4]^{2-}$ solution containing 100 equivalents of *R*-G, increasing amounts of NEt_4Cl have been added. NMR studies showed that the cage binds the achiral guest much stronger than the chiral guest. As a consequence, the more NEt_4^+ is added the more the CD signal decreases due to the exchange between chiral and achiral guests (Figure 7A). This further confirms that ICD signal arises from a host-guest recognition event. Second, to a $[Eu_2L^M_4]^{2-}$ solution containing 50 equivalents of *R*-G, increasing amounts of *S*-G have been added up to induce an opposite CD signal (Figure 7B), highlighting the adaptive behavior of the system. Third, $[Eu_2L^M_4]^{2-}$ has been tested as chiral sensor to evaluate the possibility of straightforward enantiomeric excess (*ee*) determination. A series of CD spectra were collected with varying enantiomeric compositions of the chiral guest (Figure S40), and a calibration curve was derived. The CD value at $\lambda = 349$ nm was plotted against the %*ee*, evidencing a linear relation ($R^2 = 0.999$, Figure 7C). To estimate the error in the determination of the chiral guest *ee*, four solutions with "unknown" enantiomeric composition were measured (Table S11). From these measurements, the enantiomeric excess value resulted to be determined with an average error of $\pm 3.3\%$.

The ICD experiments prove the guest-to-host chiral induction by probing the absorption bands of the ligands. However, the peculiar emission properties of the Eu-helicates allow to perform CPL experiments and probe the chiral induction to the metal coordination environment. Studies of CPL-emitting materials are gaining particular attention since they find potential applications as diagnostic tools, biological probes, and spintronic devices.[22,61] The two Eu cages were tested in presence of both enantiomers of α-methylcholine, and the CPL spectra were recorded at different guest concentrations. Since the chiral guest is not a luminophore, the CPL signal is related only to the chiral environment around the Eu^{3+}-emitting ion. As already observed in CD experiments, in absence of a primary level of chiral information, in solution the assemblies are present as a racemic mixture of the helicates, and eventually the mesocate isomers, therefore, do not show any signal in the considered spectral range (565–725 nm). However, upon addition of the chiral guests, an induced CPL signal (ICPL), related to $^5D_0 \rightarrow {}^7F_J$ ($J = 0$–4) Eu^{3+} transitions, was detected (Figure 8). As expected, the two guest enantiomers induced mirror-image CPL signals, in agreement with the CD experiments. The transitions attributed to $^5D_0 \rightarrow {}^7F_1$ and $^5D_0 \rightarrow {}^7F_2$ show the larger intensity variations (ΔI) than the other emission bands $^5D_0 \rightarrow {}^7F_J$ ($J = 0, 3, 4$). In particular, the $^5D_0 \rightarrow {}^7F_1$ transition, despite the lower total emission intensity, has a transition magnetic dipole moment that satisfies the magnetic-dipole selection rule $\Delta J = 0, \pm 1$ (except $0 \rightarrow 0$), and hence it gives large circular polarization.[58] Lunkley et al.[62] have evidenced that CPL spectra

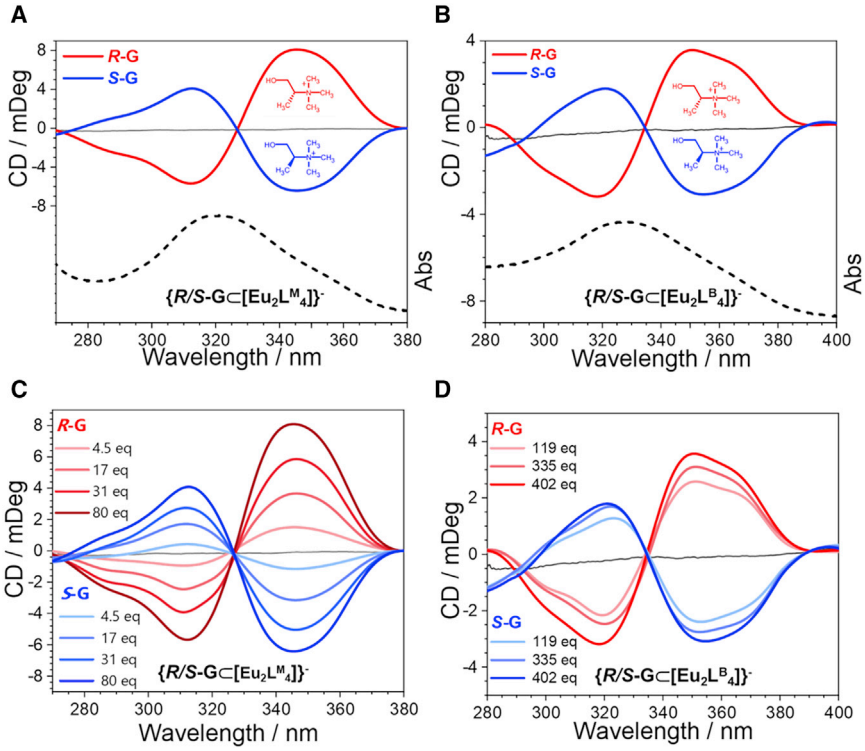

Figure 6. Induced circular dichroism (CD)

(A and B) Ultraviolet-visible (UV-vis) absorption spectra (black dashed curves) and CD spectra (red and blue curves) of the cages $[Eu_2L^M_4]^{2-}$ and $[Eu_2L^B_4]^{2-}$ solutions ($1.9 \cdot 10^{-5}$ M, CH_3CN) after the addition of 80 and 400 eq of the chiral guest (*R* or *S*), respectively. The gray lines are the CD spectra of the chiral guests (*R*-G and *S*-G).

(C and D) CD spectra at increasing chiral guest concentration (*R* or *S*) for $[Eu_2L^M_4]^{2-}$ and $[Eu_2L^B_4]^{2-}$ solutions ($1.9 \cdot 10^{-5}$ M, CH_3CN). The gray lines are the CD spectra with 0 eq of chiral guest.

can be used to draw some helicity rule to gain information about the absolute configuration of the Eu centers. In particular, a negative signal at the $^5D_0 \rightarrow {}^7F_1$ transition and a positive signal at the $^5D_0 \rightarrow {}^7F_2$ one denotes the presence of a Λ configuration around the Ln^{3+} center; conversely, the opposite situation indicates a Δ configuration. In presence of the *R*-G guest, both the Eu cages show a negative ($^5D_0 \rightarrow {}^7F_1$)-positive ($^5D_0 \rightarrow {}^7F_2$) signal (red line, Figure 8), suggesting that *R*-G has a higher affinity for the *M*-helicate (ΛΛ); conversely, in presence of the *S*-G guest, positive ($^5D_0 \rightarrow {}^7F_1$)-negative ($^5D_0 \rightarrow {}^7F_2$) CPL signal (blue line, Figure 8), the *P*-helicate (ΔΔ) is the most stable. These findings fully agree with the helicity information derived from the CD spectra. As previously done with CD, a series of experiments at different host/guest ratios were performed, focusing on the region of the most intense transitions (565–665 nm, Figures 8C and 8D; Tables S12 and S13). Again, the signal increases with the chiral guest concentration, in agreement with what was observed in the ICD experiments, and the $\{R/S\text{-G}\subset[Eu_2L^B_4]\}^-$ systems, with the more rigid ligand L^B, show lower ICPL signals for a given guest concentration. The g_{lum} curves show a typical behavior for Eu(III) β-diketonato complexes (Figures 8A and 8B).[63] The magnetically allowed transition $^5D_0 \rightarrow {}^7F_1$ displays the higher $|g_{lum}|$ value ($g_{lum} = 2\Delta I/I$) and has a rotational strength almost equal and opposite to the intense $^5D_0 \rightarrow {}^7F_2$ transition, having an electric-dipole character and therefore a much smaller g_{lum} (Figures 8A and 8B). The calculated absolute $|g_{lum}|$ values ($^5D_0 \rightarrow {}^7F_1$ transition) for the four systems are consistent with those reported in literature

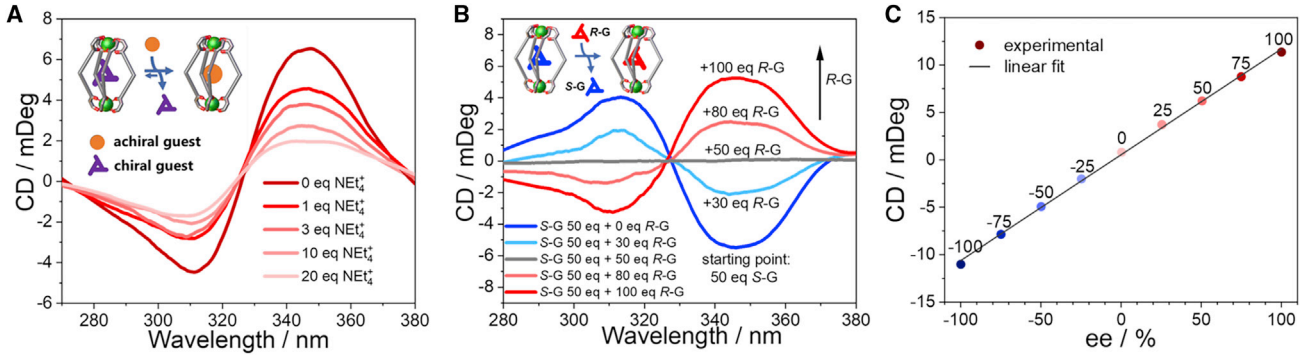

Figure 7. Chiral/achiral and chiral *S*-G/*R*-G guest exchange and %*ee* determination

(A) CD spectra of $[Eu_2L^M_4]^{2-}$ ($1.8 \cdot 10^{-5}$ M, CH_3CN) in the presence of the 100 eq of chiral guest *R*-G after the addition of different amounts of NEt_4^+ achiral guest.

(B) Exchange of *R*-G with *S*-G and adaptive behavior of the $[Eu_2L^M_4]^{2-}$.

(C) Enantiomeric excess calibration curve for straightforward enantiomeric excess determination with $[Eu_2L^M_4]^{2-}$ cage (CD values at 349 nm).

for Eu luminescent complexes ($|g_{lum}| > 10^{-2}$).[32,33,64,65] In particular, for $\{R/S\text{-G} \subset [Eu_2L^M_4]\}^-$ $g_{lum} = -0.064$(*R*-G) and 0.061(*S*-G), while for $\{R/S\text{-G} \subset [Eu_2L^B_4]\}^-$ $g_{lum} = -0.032$(*R*-G) and 0.027(*S*-G), when using the follow guest:cage ratio *R*/*S*-G:$[Eu_2L^M_4]^{2-}$ = 200:1 and *R*/*S*-G:$[Eu_2L^B_4]^{2-}$ = 400:1. Also, g_{lum} values confirmed that $[Eu_2L^M_4]^{2-}$ has a higher induced chiral response than $[Eu_2L^B_4]^{2-}$. In fact, $[Eu_2L^M_4]^{2-}$ gives $|g_{lum}|$ values that are twice that of $[Eu_2L^B_4]^{2-}$ using half of the chiral guest equivalents. It is important to notice that g_{lum} is usually defined for enantiomerically pure systems, i.e., compounds that have reached the total enrichment in one of the two enantiomers. Since the total enrichment in one of the two helicates could not be confirmed, the reported g_{lum} values can only give the order of magnitude of this factor.

Helicity inversion mechanism

SCXRD structures evidenced that $[Eu_2L^B_4]^{2-}$ and $[Eu_2L^M_4]^{2-}$ crystallize as helicates and mesocate, respectively. At the same time, both the empty cages in the presence of the chiral guest gave ICD and ICPL signals due to the asymmetric induction in the supramolecular helicity. This indicates that in solution, at least in the presence of the chiral guest, also $[Eu_2L^M_4]^{2-}$ is in the helicate form. Although helicates and mesocates have been known for some decades,[66,67] the factors that allow to drive the formation of one isomer with respect to the other are still not properly understood. Several parameters affecting the formation of helicate or mesocate have been reported, as for instance the metal ion dimensions,[68,69] the steric hindrance of the ligand,[69,70] and the spacer length (odd-even rule).[8,70] However, the same ligand and metal can lead to the formation of both the isomers.[71] Even host-guest interactions can affect the final conformer.[72–74] Moreover, we must be aware that when different (metallo)supramolecular ensembles are in equilibrium, crystallization can be a sorting factor,[75,76] allowing a quantitative selection even toward the less thermodynamically stable system. Consequently, we ran a series of DFT calculations to investigate some important factors that can influence the helicate-mesocate equilibrium in the presented cages such as (1) the ligand (L^B or L^M), (2) the presence of the guest inside the cavity, and (3) the guest nature. These calculations were useful to elucidate the conformational isomer present in solution and to propose a mechanism for the helicity inversion. Lanthanum cages were used for DFT studies since La^{3+} has a closed shell electronic configuration that allows to simplify calculations with almost negligible effects on the geometrical parameters. Geometry optimizations

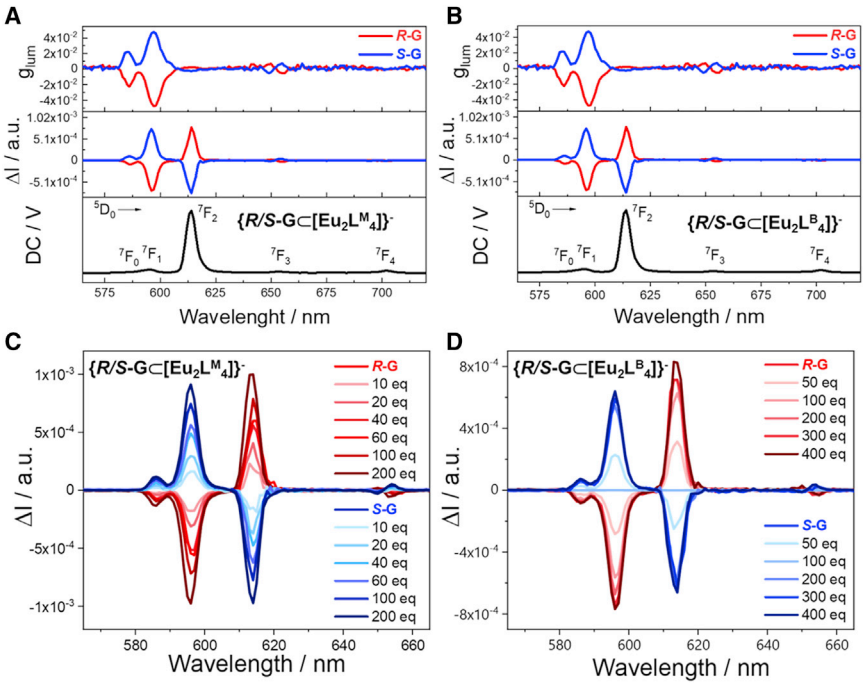

Figure 8. Induced circularly polarized luminescence (CPL)

(A and B) Photoluminescence spectra (black curves) and CPL spectra (ΔI and g_{lum}, red and blue curves) of the cages $[Eu_2L^M_4]^{2-}$ and $[Eu_2L^B_4]^{2-}$ in CH_3CN solutions ($1.0 \cdot 10^{-5}$ M) after the addition of 100 and 400 eq of the chiral guest (*R* or *S*), respectively.

(C and D) CPL spectra (ΔI) at increasing chiral guest concentration (*R* or *S*) for $[Eu_2L^M_4]^{2-}$ and $[Eu_2L^B_4]^{2-}$ in CH_3CN solutions ($1.0 \cdot 10^{-5}$ M).

were obtained with the inclusion of solvent effects and dispersion corrections (see supplemental experimental procedures for details). The empty cages and the host-guest systems (with NEt_4^+ and both *R*-G and *S*-G) were optimized in the helicate and mesocate forms. The comparison of X-ray and calculated structures for the helicate $\{NEt_4 \subset [Eu_2L^B_4]\}^-$/$\{NEt_4 \subset [La_2L^B_4]\}^-$ and the mesocate $\{NEt_4 \subset [Eu_2L^M_4]\}^-$/$\{NEt_4 \subset [La_2L^M_4]\}^-$ shows that optimized structures are in very good agreement with the experimental ones (Figure S41). Calculations showed that for cages with L^B ligand, the helicate is always the most stable isomer, with an energy difference between helicate and mesocate ($\Delta E_{h\text{-}m}$) of at least 7 kcal/mol (Figure S42; Table S14). Also, for the cages with the more flexible L^M ligand, the helicate form is always the most stable, even if the $\Delta E_{h\text{-}m}$ values are much lower (Figure S42; Table S14). In particular, for $\{NEt_4 \subset [La_2L^M_4]\}^-$ host-guest system $\Delta E_{h\text{-}m} = -1.8$ kcal/mol, corresponding to the following Boltzmann distribution at 298 K: 95% helicate and 5% mesocate. This suggests that the isolated mesocate form for $[Eu_2L^M_4]^{2-}$ single crystals may be the consequence of a selection induced by a phase change (i.e., crystallization). To summarize, DFT calculations strongly support that both the empty cages and the host-guest systems are present in solution as helicates. Moreover, optimization of the host-guest systems gave important insight on how the chiral guest allocates inside the cage cavity. Both the SCXRD structures and the DFT calculations showed that the NEt_4^+ lays on the equatorial plane of the cage cavity. Similarly, the chiral guest lays on the cavity center, but DFT calculations also highlighted that in the more stable structures it orientates inside the cavity in order to form an H-bond between its OH group and one of the oxygen atoms of the bis-β-diketonato ligands (Figure S43).

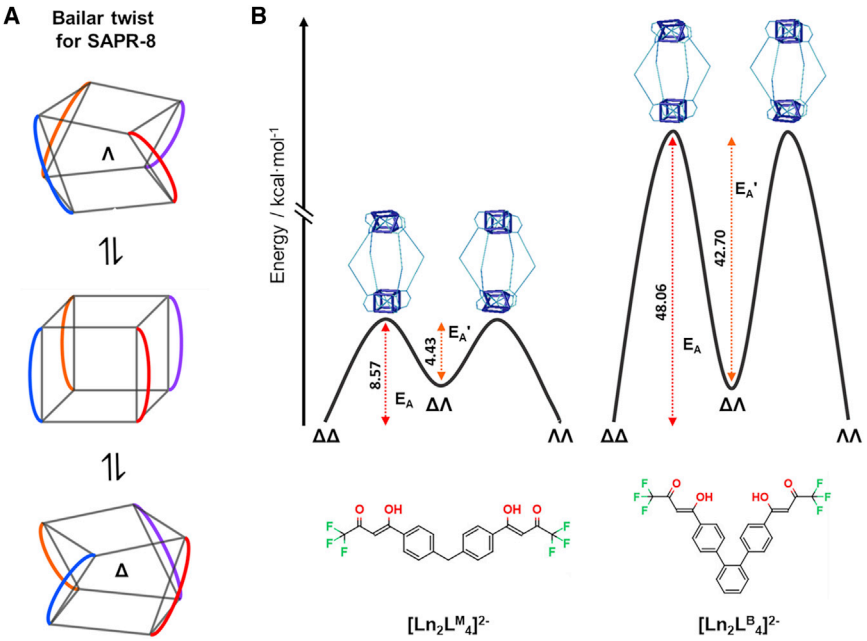

Figure 9. Helicity inversion mechanism

(A) Schematization of the Bailar twist mechanism for a mononuclear SAPR-8-chelated complex. The four chelating ligands are depicted in blue, red, orange, and purple.

(B) Helicity inversion mechanism with associated activation energies for the empty cages $[La_2L^M{}_4]^{2-}$ and $[La_2L^B{}_4]^{2-}$. The simplified transition state structures, highlighting the atoms arrangement around the metal centers, are reported in blue.

Finally, DFT calculations have been exploited to propose a helicity inversion mechanism in order also to evaluate the role of the ligand nature, in terms of scaffold flexibility, on the chiral induction. Helicity inversion can occur via inter- or intramolecular reorganization. The former mechanism requires the dissociation of at least one chelating ligand, followed by recomplexation. On the contrary, the intramolecular mechanism involves a ligand rearrangement around the metal center without their dissociation. In literature, only a few studies about the mechanism of helicates inversion or helicate-mesocate conversion are reported,[72,77,78] and in these few examples the rearrangement mechanism resulted to be intramolecular. As reported by Kersting et al.[77] and Meyer et al.[78] for the intramolecular helicity inversion of Ga triple-stranded helicates, the two metal centers twist independently from each other passing through the mesocate form as intermediate. A single metal center can invert its helicity through two possible non-dissociative processes: Bailar or Rây-Dutt twist.[79,80] Both these mechanisms were defined for octahedral complexes coordinating three bidentate chelate ligands, but can be easily extended to octa-coordinated SAPR-8 complexes. The helicity inversion in an SAPR-8 structure leads to a transition state that assumes an elongated-cubic arrangement and the point group symmetries become D_{4h} (Bailar) or C_{2v} (Rây-Dutt). In octahedral mononuclear complexes, the probability of the two mechanisms can be predicted by geometrical considerations.[79,80] In the case of dinuclear cages instead, the high distortion imposed to the cage by the Rây-Dutt twist allows to exclude this intramolecular inversion mechanism. Consequently, a Bailar twist (Figure 9A) was studied as mechanism for the helicity inversion of the empty cages via DFT calculations (Figure 9). An elongated cubic coordination geometry around the metal center that undergoes the inversion was considered as transition state for the cages $[La_2L^M{}_4]^{2-}$ and $[La_2L^B{}_4]^{2-}$. This allows to determine the activation energies of the conversion from helicate to mesocate (E_A) and vice versa (E_A') (Figure 9B). Obviously, the helicity inversion requires a two-step

process such as helicate (*P*-ΔΔ) → mesocate (ΔΛ) → helicate (*M*-ΛΛ) or vice versa. The activation energies of the two cages are very different: with the more flexible ligand L^M, the helicate → mesocate E_A is 8.6 kcal/mol, while E_A' is 4.4 kcal/mol for the mesocate → helicate rearrangement (Figure 9B). For the cage $[La_2L^B_4]^{2-}$, these two energies are five times (E_A = 48.1 kcal/mol) and ten times (E_A' = 42.7 kcal/mol) higher than $[La_2L^M_4]^{2-}$, respectively (Figure 9B). This suggests that the helicity inversion should be much more favored for the cage synthesized with the flexible ligand (L^M), with respect to the rigid one (L^B) as actually evidenced by ICD and ICPL experiments.

In conclusion, we reported the design, synthesis, and characterization $[Ln_2L_4]^{2-}$ quadruple-stranded helicate-cages present in solution as a racemic mixture of left- and right-handed helicates, in dynamic equilibrium. Interaction with chiral α-methylcholine guests shifts the equilibrium thanks to a guest-to-host chiral induction, resulting in the enrichment of either the *M*- or *P*-helicate. The guests, having chirality at a primary level, transfer the chiral information to a metallo-supramolecular ensemble (the helicate) composed of achiral components, and therefore manifest chirality at a secondary level. The helicity asymmetrization was followed with a chiroptical readout in both absorption and emission. The absorption bands of the ligands allow to study the system via CD, while the peculiar Eu cages' emission properties give access to CPL spectroscopy. Both techniques confirmed that the *R* enantiomer of the chiral guest stabilizes the *M* (ΛΛ) helicate, while the *S* enantiomer the *P* (ΔΔ) configuration. Moreover, ICD and ICPL experiments clearly evidenced that the more flexible $[Eu_2L^M_4]^{2-}$ has a higher "chiral response" than the more rigid $[Eu_2L^B_4]^{2-}$ and can find applications for straightforward and precise enantiomeric excess determination, as evidenced for the *ee* determination of α-methylcholine. Adaptive chiral response is induced by the host-guest interaction; hence, it depends on the host-guest affinity. NMR analysis allows to determine the association constants of the cages with chiral and achiral cationic guests, confirming in both cases a higher affinity for $[Ln_2L^M_4]^{2-}$ rather than $[Ln_2L^B_4]^{2-}$. In addition, the study of the helicity inversion mechanism, as intramolecular Bailar twist, strongly supports the hypothesis that the chiral response is also affected by the ligand scaffold flexibility. Indeed, the nature of the ligand is reflected in terms of the activation energy barriers for helical rearrangements. This last result allows to draw a sort of guideline for the design of new dynamic and adaptive chiral systems based on helicates. To enhance the hierarchical chiral transfer, arising from supramolecular interactions such as host-guest properties, the design of systems with good host-guest affinities is necessary, but the use of ligands with quite flexible scaffolds appears to also be of paramount importance. We envision that lanthanide helicates endowed with peculiar chirality, emission, and host-guest properties will foster the development of optical probes for highly selective chiral sensing able to convert the molecular recognition events in an easy to measure chiroptical output (i.e., CD and CPL).

EXPERIMENTAL PROCEDURES

Resource availability

Lead contact

Further information and requests for resources should be directed to and will be fulfilled by the lead contact, Marzio Rancan (marzio.rancan@cnr.it or marzio.rancan@unipd.it).

Materials availability

Commercially available reagents were used without further purification. Detailed procedures can be found in the supplemental experimental procedures.

Data and code availability

The accession numbers for the crystallographic data reported in this paper are CCDC 2072562-2072565. Copies of these data can be obtained free of charge from the Cambridge Crystallographic Data Centre (CCDC) via https://www.ccdc.cam.ac.uk:443/data_request/cif. Correspondence and requests for materials should be addressed to M.R.

SUPPLEMENTAL INFORMATION

Supplemental information can be found online at https://doi.org/10.1016/j.xcrp.2021.100692.

ACKNOWLEDGMENTS

This work was funded by the University of Padova (grant P-DISC #CARL-SID17 BIRD2017-UNIPD, Project CHIRoN) and by Deutsche Forschungsgemeinschaft (DFG [German Research Foundation]) under Germany's Excellence Strategy—EXC 2033–390677874—RESOLV and GRK2376 "Confinement-controlled Chemistry"—project 331085229.

AUTHOR CONTRIBUTIONS

M.R. conceived the project. M.R., J.T., A.C., M.R., L.B., and E.B. performed the synthesis and NMR characterization. R.S. performed MS analysis. G.B. performed the photophysical studies. A.C. and L.B. performed CD spectroscopy. J.T. and A.C. performed CPL analysis. M.R. collected the X-ray data and solved and refined the structures. S.C. performed the DFT calculations. L.A., M.C., and G.H.C. put forward many constructive suggestions on the experimental design. M.R. and J.T. drafted the manuscript. All authors contributed to the analysis of the results and the writing of the manuscript.

DECLARATION OF INTERESTS

The authors declare no competing interests.

Received: July 1, 2021
Revised: November 8, 2021
Accepted: November 19, 2021
Published: December 10, 2021

REFERENCES

1. Morrow, S.M., Bissette, A.J., and Fletcher, S.P. (2017). Transmission of chirality through space and across length scales. Nat. Nanotechnol. *12*, 410–419.

2. Baron, M., Rancan, M., Armelao, L., and Tubaro, C. (2021). Quantitative Selection of the Axially Chiral Conformation in a Flexible Dinuclear Gold(I) di(N-Heterocyclic Carbene) Complex via Chlorine Oxidative Addition. J. Chem. Crystallogr. *51*, 175–182.

3. Rancan, M., and Armelao, L. (2015). Exploiting dimensional variability in coordination polymers: solvent promotes reversible conversion between 3D and chiral 1D architectures. Chem. Commun. (Camb.) *51*, 12947–12949.

4. Yan, Z.H., Li, D., and Yin, X.B. (2017). Review for chiral-at-metal complexes and metal-organic framework enantiomorphs. Sci. Bull. (Beijing) *62*, 1344–1354.

5. Albrecht, M. (2001). "Let's twist again"–double-stranded, triple-stranded, and circular helicates. Chem. Rev. *101*, 3457–3497.

6. Albrecht, M. (2005). Supramolecular Templating in the Formation of Helicates (Springer), pp. 105–139.

7. Lehn, J.-M., Rigault, A., Siegel, J., Harrowfield, J., Chevrier, B., and Moras, D. (1987). Spontaneous assembly of double-stranded helicates from oligobipyridine ligands and copper(I) cations: structure of an inorganic double helix. Proc. Natl. Acad. Sci. USA *84*, 2565–2569.

8. Albrecht, M. (2000). How do they know? Influencing the relative stereochemistry of the complex units of dinuclear triple-stranded helicate-type complexes. Chemistry *6*, 3485–3489.

9. Yeh, R.M., Ziegler, M., Johnson, D.W., Terpin, A.J., and Raymond, K.N. (2001). Imposition of chirality in a dinuclear triple-stranded helicate by ion pair formation. Inorg. Chem. *40*, 2216–2217.

10. Yeh, R.M., and Raymond, K.N. (2006). Supramolecular asymmetric induction in dinuclear triple-stranded helicates. Inorg. Chem. *45*, 1130–1139.

11. Haino, T., Shio, H., Takano, R., and Fukazawa, Y. (2009). Asymmetric induction of supramolecular helicity in calix[4]arene-based triple-stranded helicate. Chem. Commun. (Camb.) *2481–2483*, 2481–2483.

12. Ikeda, A., Udzu, H., Zhong, Z., Shinkai, S., Sakamoto, S., and Yamaguchi, K. (2001). A

self-assembled homooxacalix[3]arene-based dimeric capsule constructed by a Pd(II)-pyridine interaction which shows a novel chiral twisting motion in response to guest inclusion. J. Am. Chem. Soc. *123*, 3872–3877.

13. Regeni, I., Chen, B., Frank, M., Baksi, A., Holstein, J.J., and Clever, G.H. (2021). Coal-Tar Dye-based Coordination Cages and Helicates. Angew. Chem. Int. Ed. Engl. *60*, 5673–5678.

14. Li, R.J., Holstein, J.J., Hiller, W.G., Andréasson, J., and Clever, G.H. (2019). Mechanistic Interplay between Light Switching and Guest Binding in Photochromic [Pd_2Dithienylethene$_4$] Coordination Cages. J. Am. Chem. Soc. *141*, 2097–2103.

15. Yang, D., von Krbek, L.K.S., Yu, L., Ronson, T.K., Thoburn, J.D., Carpenter, J.P., Greenfield, J.L., Howe, D.J., Wu, B., and Nitschke, J.R. (2021). Glucose Binding Drives Reconfiguration of a Dynamic Library of Urea-Containing Metal-Organic Assemblies. Angew. Chem. Int. Ed. Engl. *60*, 4485–4490.

16. Wong, H.Y., Lo, W.S., Yim, K.H., and Law, G.L. (2019). Chirality and Chiroptics of Lanthanide Molecular and Supramolecular Assemblies. Chem *5*, 3058–3095.

17. Wu, T., Bouř, P., and Andrushchenko, V. (2019). Europium (III) as a Circularly Polarized Luminescence Probe of DNA Structure. Sci. Rep. *9*, 1068.

18. Han, J., Guo, S., Lu, H., Liu, S., Zhao, Q., and Huang, W. (2018). Recent Progress on Circularly Polarized Luminescent Materials for Organic Optoelectronic Devices. Adv. Opt. Mater. *6*, 1800538.

19. Carr, R., Evans, N.H., and Parker, D. (2012). Lanthanide complexes as chiral probes exploiting circularly polarized luminescence. Chem. Soc. Rev. *41*, 7673–7686.

20. Heffern, M.C., Matosziuk, L.M., and Meade, T.J. (2014). Lanthanide probes for bioresponsive imaging. Chem. Rev. *114*, 4496–4539.

21. Kitagawa, Y., Tsurui, M., and Hasegawa, Y. (2020). Steric and Electronic Control of Chiral Eu(III) Complexes for Effective Circularly Polarized Luminescence. ACS Omega *5*, 3786–3791.

22. Muller, G. (2009). Luminescent chiral lanthanide(III) complexes as potential molecular probes. Dalt. Trans. *2009*, 9692–9707.

23. Bradberry, S.J., Savyasachi, A.J., Martinez-Calvo, M., and Gunnlaugsson, T. (2014). Development of responsive visibly and NIR luminescent and supramolecular coordination self-assemblies using lanthanide ion directed synthesis. Coord. Chem. Rev. *273–274*, 226–241.

24. Song, H., Postings, M., Scott, P., and Rogers, N.J. (2021). Metallohelices emulate the properties of short cationic α-helical peptides. Chem. Sci. (Camb.) *12*, 1620–1631.

25. Howson, S.E., Bolhuis, A., Brabec, V., Clarkson, G.J., Malina, J., Rodger, A., and Scott, P. (2011). Optically pure, water-stable metallo-helical 'flexicate' assemblies with antibiotic activity. Nat. Chem. *4*, 31–36.

26. Zhao, C., Song, H., Scott, P., Zhao, A., Tateishi-Karimata, H., Sugimoto, N., Ren, J., and Qu, X. (2018). Mirror-Image Dependence: Targeting Enantiomeric G-Quadruplex DNA Using Triplex Metallohelices. Angew. Chem. Int. Ed. Engl. *57*, 15723–15727.

27. Oleksy, A., Blanco, A.G., Boer, R., Usón, I., Aymamí, J., Rodger, A., Hannon, M.J., and Coll, M. (2006). Molecular recognition of a three-way DNA junction by a metallosupramolecular helicate. Angew. Chem. Int. Ed. Engl. *45*, 1227–1231.

28. Schoentjes, B., and Lehn, J.-M. (1995). Interaction of Double-Helical Polynuclear Copper(I) complexes with double-stranded DNA. Helv. Chim. Acta *78*, 1–12.

29. Guo, X.-Q., Zhou, L.-P., Hu, S.-J., Cai, L.-X., Cheng, P.-M., and Sun, Q.-F. (2021). Hexameric Lanthanide–Organic Capsules with Tertiary Structure and Emergent Functions. J. Am. Chem. Soc. *29*, jacs.1c01168.

30. Yeung, C.T., Chan, W.T.K., Yan, S.C., Yu, K.L., Yim, K.H., Wong, W.T., and Law, G.L. (2015). Lanthanide supramolecular helical diastereoselective breaking induced by point chirality: mixture or *P*-helix, *M*-helix. Chem. Commun. (Camb.) *51*, 592–595.

31. Cai, L.X., Yan, L.L., Li, S.C., Zhou, L.P., and Sun, Q.F. (2018). Stereocontrolled self-assembly and photochromic transformation of lanthanide supramolecular helicates. Dalton Trans. *47*, 14204–14210.

32. Zhou, Y., Yao, Y., Cheng, Z., Gao, T., Li, H., and Yan, P. (2020). Point Chirality Controlled Diastereoselective Self-Assembly and Circularly Polarized Luminescence in Quadruple-Stranded Europium(III) Helicates. Inorg. Chem. *59*, 12850–12857.

33. Han, G., Zhou, Y., Yao, Y., Cheng, Z., Gao, T., Li, H., and Yan, P. (2020). Preorganized helical chirality controlled homochiral self-assembly and circularly polarized luminescence of a quadruple-stranded Eu_2L_4 helicate. Dalton Trans. *49*, 3312–3320.

34. Sahoo, J., Arunachalam, R., Subramanian, P.S., Suresh, E., Valkonen, A., Rissanen, K., and Albrecht, M. (2016). Coordinatively Unsaturated Lanthanide(III) Helicates: Luminescence Sensors for Adenosine Monophosphate in Aqueous Media. Angew. Chem. Int. Ed. Engl. *55*, 9625–9629.

35. Yao, Z., Zhou, Y., Gao, T., Yan, P., and Li, H. (2021). Ancillary ligand modulated stereoselective self-assembly of triple-stranded Eu(III) helicate featuring circularly polarized luminescence. RSC Adv. *11*, 10524–10531.

36. Zhang, Z., Zhou, Y., Gao, T., Yan, P., Zou, X., and Li, H. (2021). Diastereoselective self-assembly of a triple-stranded europium helicate with light modulated chiroptical properties. Dalton Trans. *50*, 4604–4612.

37. Suko, N., Itamoto, H., Okayasu, Y., Okura, N., and Yuasa, J. (2021). Helix-mediated over 1 nm-range chirality recognition by ligand-to-ligand interactions of dinuclear helicates. Chem. Sci. (Camb.) *12*, 8746–8754.

38. Bing, T.Y., Kawai, T., and Yuasa, J. (2018). Ligand-to-Ligand Interactions That Direct Formation of D_2-Symmetrical Alternating Circular Helicate. J. Am. Chem. Soc. *140*, 3683–3689.

39. Tan, Y.B., Okayasu, Y., Katao, S., Nishikawa, Y., Asanoma, F., Yamada, M., Yuasa, J., and Kawai, T. (2020). Visible Circularly Polarized Luminescence of Octanuclear Circular Eu(III) Helicate. J. Am. Chem. Soc. *142*, 17653–17661.

40. Stomeo, F., Lincheneau, C., Leonard, J.P., O'Brien, J.E., Peacock, R.D., McCoy, C.P., and Gunnlaugsson, T. (2009). Metal-directed synthesis of enantiomerially pure dimetallic lanthanide luminescent triple-stranded helicates. J. Am. Chem. Soc. *131*, 9636–9637.

41. Albrecht, M., Schmid, S., Dehn, S., Wickleder, C., Zhang, S., Bassett, A.P., Pikramenou, Z., and Fröhlich, R. (2007). Diastereoselective formation of luminescent dinuclear lanthanide(III) helicates with enantiomerically pure tartaric acid derived bis(β- diketonate) ligands. New J. Chem. *31*, 1755–1762.

42. Lincheneau, C., Peacock, R.D., and Gunnlaugsson, T. (2010). Europium directed synthesis of enantiomerically pure dimetallic luminescent "squeezed" triple-stranded helicates; solution studies. Chem. Asian J. *5*, 500–504.

43. Kotova, O., Comby, S., Pandurangan, K., Stomeo, F., O'Brien, J.E., Feeney, M., Peacock, R.D., McCoy, C.P., and Gunnlaugsson, T. (2018). The effect of the linker size in C_2-symmetrical chiral ligands on the self-assembly formation of luminescent triple-stranded di-metallic Eu(iii) helicates in solution. Dalton Trans. *47*, 12308–12317.

44. Li, X.Z., Zhou, L.P., Yan, L.L., Yuan, D.Q., Lin, C.S., and Sun, Q.F. (2017). Evolution of Luminescent Supramolecular Lanthanide $M_{2n}L_{3n}$ Complexes from Helicates and Tetrahedra to Cubes. J. Am. Chem. Soc. *139*, 8237–8244.

45. Barry, D.E., Caffrey, D.F., and Gunnlaugsson, T. (2016). Lanthanide-directed synthesis of luminescent self-assembly supramolecular structures and mechanically bonded systems from acyclic coordinating organic ligands. Chem. Soc. Rev. *45*, 3244–3274.

46. Barry, D.E., Kitchen, J.A., Pandurangan, K., Savyasachi, A.J., Peacock, R.D., and Gunnlaugsson, T. (2020). Formation of Enantiomerically Pure Luminescent Triple-Stranded Dimetallic Europium Helicates and Their Corresponding Hierarchical Self-Assembly Formation in Protic Polar Solutions. Inorg. Chem. *59*, 2646–2650.

47. Kredel, S., Nienhaus, K., Oswald, F., Wolff, M., Ivanchenko, S., Cymer, F., Jeromin, A., Michel, F.J., Spindler, K.D., Heilker, R., et al. (2008). Optimized and far-red-emitting variants of fluorescent protein eqFP611. Chem. Biol. *15*, 224–233.

48. Butler, S.J., McMahon, B.K., Pal, R., Parker, D., and Walton, J.W. (2013). Bright mono-aqua europium complexes based on triazacyclononane that bind anions reversibly and permeate cells efficiently. Chemistry *19*, 9511–9517.

49. Montgomery, C.P., Murray, B.S., New, E.J., Pal, R., and Parker, D. (2009). Cell-penetrating metal complex optical probes: targeted and

responsive systems based on lanthanide luminescence. Acc. Chem. Res. *42*, 925–937.

50. Bottaro, G., Rizzo, F., Cavazzini, M., Armelao, L., and Quici, S. (2014). Efficient luminescence from fluorene- and spirobifluorene-based lanthanide complexes upon near-visible irradiation. Chemistry *20*, 4598–4607.

51. Lima, P.P., Sá Ferreira, R.A., Freire, R.O., Almeida Paz, F.A., Fu, L., Alves, S., Jr., Carlos, L.D., and Malta, O.L. (2006). Spectroscopic study of a UV-photostable organic-inorganic hybrids incorporating an Eu3+ β-diketonate complex. ChemPhysChem *7*, 735–746.

52. Truccolo, G., Tessari, Z., Tessarolo, J., Quici, S., Armelao, L., and Rancan, M. (2018). A Cu(ii) metallocycle for the reversible self-assembly of coordination-driven polyrotaxane-like architectures. Dalton Trans. *47*, 12079–12084.

53. Casanova, D., Llunell, M., Alemany, P., and Alvarez, S. (2005). The rich stereochemistry of eight-vertex polyhedra: a continuous shape measures study. Chemistry *11*, 1479–1494.

54. Binnemans, K. (2015). Interpretation of europium(III) spectra. Coord. Chem. Rev. *295*, 1–45.

55. Caulder, D.L., and Raymond, K.N. (1999). The rational design of high symmetry coordination clusters. Dalt. Trans. *1999*, 1185–1200.

56. Binnemans, K. (2005). Rare-earth beta-diketonates. Handb. Phys. Chem. Rare Earths *35*, 107–272.

57. Carlotto, A., Babetto, L., Carlotto, S., Miozzi, M., Seraglia, R., Casarin, M., Bottaro, G., Rancan, M., and Armelao, L. (2020). Luminescent Thermometers: From a Library of Europium(III) β-Diketonates to a General Model for Predicting the Thermometric Behaviour of Europium-Based Coordination Systems. ChemPhotoChem *4*, 674–684.

58. Tor, Y., Shanzer, A., and Scherz, A. (1990). Geometries of Non-Transition-Metal Complexes of a Novel Chiral β-Keto Amide Tripodal Ligand Elucidated from the Optical Transitions to Excitonic States. Inorg. Chem. *29*, 4096–4099.

59. Telfer, S.G., McLean, T.M., and Waterland, M.R. (2011). Exciton coupling in coordination compounds. Dalton Trans. *40*, 3097–3108.

60. Berova, N., Di Bari, L., and Pescitelli, G. (2007). Application of electronic circular dichroism in configurational and conformational analysis of organic compounds. Chem. Soc. Rev. *36*, 914–931.

61. Longhi, G., Castiglioni, E., Koshoubu, J., Mazzeo, G., and Abbate, S. (2016). Circularly Polarized Luminescence: A Review of Experimental and Theoretical Aspects. Chirality *28*, 696–707.

62. Lunkley, J.L., Shirotani, D., Yamanari, K., Kaizaki, S., and Muller, G. (2011). Chiroptical spectra of a series of tetrakis((+)-3-heptafluorobutylyrylcamphorato)lanthanide(III) with an encapsulated alkali metal ion: circularly polarized luminescence and absolute chiral structures for the Eu(III) and Sm(III) complexes. Inorg. Chem. *50*, 12724–12732.

63. Zinna, F., Resta, C., Abbate, S., Castiglioni, E., Longhi, G., Mineo, P., and Di Bari, L. (2015). Circularly polarized luminescence under near-UV excitation and structural elucidation of a Eu complex. Chem. Commun. (Camb.) *51*, 11903–11906.

64. Lunkley, J.L., Shirotani, D., Yamanari, K., Kaizaki, S., and Muller, G. (2008). Extraordinary circularly polarized luminescence activity exhibited by cesium tetrakis(3-heptafluoro-butylryl-(+)-camphorato) Eu(III) complexes in EtOH and $CHCl_3$ solutions. J. Am. Chem. Soc. *130*, 13814–13815.

65. Zinna, F., and Di Bari, L. (2015). Lanthanide circularly polarized luminescence: bases and applications. Chirality *27*, 1–13.

66. Lehn, J.-M. (1995). Supramolecular Chemistry: Concepts and Perspectives (Wiley).

67. Jonathan, W., and Steed, J.L.A. (2009). Supramolecular Chemistry, Second Edition (Wiley).

68. Wu, D., Huang, P., Shui, Y., and Wu, G. (2013). Coordination assembly of helicate and mesocate with two-armed carbohydrozine ligand: Synthesis, structure and fluorescence. Inorg. Chem. Commun. *29*, 205–209.

69. Cooke, D.J., Cross, J.M., Fennessy, R.V., Harding, L.P., Rice, C.R., and Slater, C. (2013). Steric control of the formation of dinuclear double helicate and dinuclear meso-helicate assemblies. Chem. Commun. (Camb.) *49*, 7785–7787.

70. Díaz, D.E., Llanos, L., Arce, P., Lorca, R., Guerrero, J., Costamagna, J., Aravena, D., Ferraudi, G., Oliver, A., Lappin, A.G., and Lemus, L. (2018). Steric and Electronic Factors Affecting the Conformation of Bimetallic Cu^{I} Complexes: Effect of the Aliphatic Spacer of Tetracoordinating Schiff-Base Ligands. Chemistry *24*, 13839–13849.

71. Zhang, Z., and Dolphin, D. (2009). A triple-stranded helicate and mesocate from the same metal and ligand. Chem. Commun. (Camb.) *2*, 6931–6933.

72. Xu, J., Parac, T.N., and Raymond, K.N. (1999). meso myths: What drives assembly of helical versus *meso*-$[M_2L_3]$ clusters? Angew. Chem. Int. Ed. Engl. *38*, 2878–2882.

73. Lin, Q., Gao, L., Kauffmann, B., Zhang, J., Ma, C., Luo, D., and Gan, Q. (2018). Helicity adaptation within a quadruply stranded helicate by encapsulation. Chem. Commun. (Camb.) *54*, 13447–13450.

74. Cui, F., Li, S., Jia, C., Mathieson, J.S., Cronin, L., Yang, X.J., and Wu, B. (2012). Anion-dependent formation of helicates versus mesocates of triple-stranded M_2L_3 ($M = Fe^{2+}$, Cu^{2+}) complexes. Inorg. Chem. *51*, 179–187.

75. Rancan, M., Tessarolo, J., Zanonato, P.L., Seraglia, R., Quici, S., and Armelao, L. (2013). Self-assembly of a constitutional dynamic library of Cu(II) coordination polygons and reversible sorting by crystallization. Dalton Trans. *42*, 7534–7538.

76. Markwell-Heys, A.W., Schneider, M.L., Madridejos, J.M.L., Metha, G.F., and Bloch, W.M. (2021). Self-sorting of porous $Cu_4L_2L'_2$ metal-organic cages composed of isomerisable ligands. Chem. Commun. (Camb.) *57*, 2915–2918.

77. Kersting, B., Meyer, M., Powers, R.E., and Raymond, K.N. (1996). Dinuclear catecholate helicates: Their inversion mechanism. J. Am. Chem. Soc. *118*, 7221–7222.

78. Meyer, M., Kersting, B., Powers, R.E., and Raymond, K.N. (1997). Rearrangement Reactions in Dinuclear Triple Helicates. Inorg. Chem. *36*, 5179–5191.

79. Rodger, A., and Johnson, B.F.G. (1988). Which Is More Likely: The Ray-Dutt Twist or the Bailar Twist? Inorg. Chem. *27*, 3061–3062.

80. Rzepa, H.S., and Cass, M.E. (2007). In search of the Bailar and Rây-Dutt twist mechanisms that racemize chiral trischelates: a computational study of Sc(III), Ti(IV), Co(III), Zn(II), Ga(III), and Ge(IV) complexes of a ligand analogue of acetylacetonate. Inorg. Chem. *46*, 8024–8031.